Photoelectrochemical CO2 reduction by a p-type boron-doped g-C3N4 electrode under visible light

doi: info:doi/10.1016/j.apcatb.2016.03.055

Photoelectrochemical CO_2 reduction by a p-type boron-doped g-C_3N_4 electrode under visible light

Nobuhiro Sagara[a], Sunao Kamimura[a,b], Toshiki, Tsubota[a], Teruhisa Ohno [a,b,c,*]

[a] Department of Materials Science, Faculty of Engineering, Kyushu Institute of Technology, 1-1 Sensuicho, Tobata, Kitakyushu 804-8550, Japan

[b] Research Center for Advanced Eco-fitting Technology, Kyushu Institute of Technology, 1-1 Sensuicho, Tobata, Kitakyushu 804-8550, Japan

[c] JST, ACT-C, 4-1-8 Honcho Kawaguchi, Saitama 332-0012, Japan

* CORRESPONDING AUTHOR

Tel.: +81 93 884 3318; fax: +81 93 884 3318

TEL & FAX: +81-93-884-3318, EMAIL ADDRESS: tohno@che.kyutech.ac.jp

Abstract

Graphitic carbon nitride (g-C_3N_4) has attracted much attention as a metal-free semiconductor having visible light absorption and relatively high chemical stability under visible light irradiation. Graphitic carbon nitride (g-C_3N_4) and boron-doped g-C_3N_4 (B-doped g-C_3N_4, BCNx) were prepared by heating melamine and a mixture of dicyanodiamide and BH_3NH_3, respectively. X-ray diffraction, a Brunauer, Emmett and Teller (BET) apparatus, and UV-vis spectra were used to analyze the physical properties of the prepared samples. Electrodes of these samples were prepared by using the electrophoresis method. X-ray photoelectron spectroscopy analyses confirmed the incorporation of boron atoms in the g-C_3N_4 framework as well as the amount of boron atoms.

Au, Ag or Rh as a co-catalyst was coated on the surface of g-C_3N_4 and B-doped g-C_3N_4 by using the magnetron sputtering method. The photocurrent response was observed using a solar simulator as a light source. The photocurrent response of B-doped g-C_3N_4 was about 5-times larger than that of pure g-C_3N_4. B-doped g-C_3N_4 coated with Rh as a co-catalyst showed the highest photocurrent response under solar light irradiation, its photocurrent being about 10-times larger than that of original g-C_3N_4. Under photoelectrochemical conditions, we also observed the products in gas phase and aqueous phase. C_2H_5OH was observed as a main product, while small amounts of CO and H_2 were observed in gas phase. We also discuss the relationship between co-catalysts and photocurrent responses and the carbon source of

C_2H_5OH as a main product. The source of carbon of C_2H_5OH obtained by CO_2 reduction is discussed on the basis of results of a labeling experiment using $^{13}CO_2$.

Keywords: Graphitic carbon nitride; Boron doping; Reduction of Carbon Dioxide; Co-catalyst-coated B-doped g-C_3N_4

1. Introduction

Carbon dioxide (CO_2) is one of the major compounds responsible for climate change, which has now become a global environmental issue because the use of huge amounts of fossil fuels consumption such as coal, crude oil, natural gas and shale oil is expected cause a drastic increase in the atmospheric CO_2 concentration in the near future [1].

Recycling of CO_2 via photoconversion to fuels such as CO, HCOOH, CH_3OH, C_2H_5OH, and CH_4 is a promising strategy for achieving a sustainable alternative to conventional fossil fuels. The development of new systems using photon energy for CO_2 reduction, which contain new photocatalysts having potential high-energy photogenerated electrons under solar light, is necessary. Various photocatalytic CO_2 reduction systems including metal complex photocatalysts [2−4], semiconductor nanomaterials [5−7] and photoelectrodes [8,9] have been reported. Semiconductor photoelectrodes are promising systems for producing valuable multiple-electron reduced products of CO_2 because they have shown to produce relatively high yields of methanol and formaldehyde [10,11]. Furthermore, development of a CO_2 conversion system using effective utilization of solar energy will be a promising solution not only for energy issues but also for overcoming the problems caused by climate change [12]. Actually, photocatalytic reaction over semiconductor photocatalysts has the potential to reduce CO_2 into valuable fuels such as CO, HCOOH, CH_3OH and CH_4 using water as an electron donor. Inoue and coworkers first reported photocatalytic CO_2 reduction in a semiconductor aqueous suspension to produce hydrocarbon fuels including

formaldehyde (HCHO), formic acid (HCOOH), methanol (CH_3OH), and methane (CH_4) [13]. However, most of the photocatalytic CO_2 reductions using metal oxide semiconductor photocatalysts are carried out under UV-light irradiation and their quantum yields for photocatalytic CO_2 reduction have been quite low. In addition, the carbon source of the products is not clear in most cases, and the synthetic process and recipe of the photocatalysts are complicated. Therefore, visible-light-driven materials with high degree of efficiency and stability represent a central challenge in the field of photocatalytic CO_2 conversion for energy-oriented use. In addition, titanium(IV) oxide(TiO_2) can produce formic acid (HCOOH), formaldehyde (HCHO), methanol (CH_3OH), and methane (CH_4) [14–26]. However, quantum yields for photocatalytic CO_2 reduction have been low and UV irradiation is necessary.

Recently, a graphitic carbon nitride (g-C_3N_4) photocatalyst with high levels of reduction ability and visible light sensitivity has attracted much attention since not only proton reduction to generate hydrogen from water but also reduction of CO_2 over g-C_3N_4 photocatalyst systems has been reported under visible-light irradiation in the presence of sacrificial reagents [27-30] Many efforts have been made to synthesize g-C_3N_4 through thermal treatment of some nitrogen-rich organic precursors, such as cyanamid, dicyanamide, triazine and heptazine derivatives [30-37]. The band gap and flat-band potential of g-C_3N_4 were reported to be 2.67 eV and −1.42 V, respectively (versus Ag/AgCl, pH 6.6) [26]. The flat band potential should be sufficient to reduce CO_2.

$CO_2 + 2H^+ + 2e^- \rightarrow HCOOH$	$E^0 = -0.57$ V (at pH 6.6 vs. NHE)
$CO_2 + 2H^+ + 2e^- \rightarrow CO + H_2O$	$E^0 = -0.52$ V (at pH 6.6 vs. NHE)
$CO_2 + 4H^+ + 4e^- \rightarrow HCHO$	$E^0 = -0.48$ V (at pH 6.6 vs. NHE)
$CO_2 + 6H^+ + 6e^- \rightarrow CH_3OH + H_2O$	$E^0 = -0.38$ V (at pH 6.6 vs. NHE)
$CO_2 + 8H^+ + 8e^- \rightarrow CH_4 + 2H_2O$	$E^0 = -0.24$ V (at pH 6.6 vs. NHE)
$2CO_2 + 12H^+ + 12e^- \rightarrow C_2H_5OH + 3H_2O$	$E^0 = 0.08$ V (at pH 6.6 vs. NHE)

However, the photocatalytic activity of g-C_3N_4 for CO_2 reduction is relatively low in most cases because of the low efficiency of oxidation of water as a counter reaction due to its low oxidation potential. In addition, g-C_3N_4 is an n-type semiconductor for which the property is not suitable for CO_2 reduction. Anion doping materials such as B-doped, P-doped, and S-doped g-C_3N_4 for improvement of photocatalytic activities have also been reported by many researchers [38-42].

In this study, we fabricated thin film electrodes of g-C_3N_4 doped with or not doped with boron atoms by an electrophoresis deposition method. The surfaces of the thin film electrodes were modified by several kinds of co-catalysts including Au, Ag and Rh by magnetron sputtering for enhancement of CO_2 reduction. The relationship between co-catalyst and product composition was examined. The carbon source of CO_2 reduction products was analyzed by a labeling experiment using $^{13}CO_2$ as a starting compound.

2. Experimental

2.1. Materials

g-C_3N_4 powder was prepared by heat treatment of melamine (Wako Pure Chemical Industries, Ltd., 99%). A typical preparation process was as follows. Melamine in an alumina pot was heated at 550 °C for 4 h in a muffle furnace [43]. Synthetic procedures for boron-doped g-C_3N_4 have been carried out by directly incorporating different amounts of BH_3NH_3 into the classical carbon nitride condensation (The resulting samples are denoted as CNBx, x= atom% of boron.) [39].

In a typical synthetic procedure, BH_3NH_3 was dissolved in water and stirred for 5 min. Then dicyandiamide was added to the aqueous solution and the mixture was heated in an oil bath at 80 °C until the water was removed and a white solid was formed. The white solid was then transferred into a crucible and heated for 4 h to reach a temperature of 600 °C and tempered at that temperature for 4 h under high purity nitrogen with a flow rate of 500 ml min^{-1}. The sample was then allowed to cool in the oven to room temperature.

Deuterium oxide, melamine, dicyandiamide, and BH_3NH_3 were purchased from Wako Pure Chemical Industries, Ltd. $^{13}CH_3{}^{13}CH_2OH$ was obtained from ISOTEC. Other chemicals were obtained from commercial sources as guaranteed reagents and were used without further purification. An FTO conductive glass substrate was obtained from AGC Fabric Co. Ltd. $^{13}CO_2$ was purchased from Science Co. Ltd.

Thin film electrodes of g-C_3N_4 doped with or not doped with boron atoms were deposited on the surfaces of FTO glass substrates by the electrophoresis method. The distance between the electrodes was fixed at 13 mm. Electrophoresis treatments was performed for 3 min with a current at 5 mA in acetone with 3 mM of I_2. After fabricating, the thin film electrodes were calcined at 300 °C for 1 h. Co-catalysts including Au, Ag, Cu and Rh were loaded on the surfaces of the prepared thin film electrodes of g-C_3N_4 doped with or not doped with boron atoms by magnetron sputtering treatment (SANYU ELECTRON Co. Ltd.).

2.2. Characterization

The crystalline phase of g-C_3N_4 and boron-doped g-C_3N_4 powders and the electrodes of g-C_3N_4 doped with or not doped with boron atoms were characterized by using a powder X-ray diffraction (XRD) instrument (MiniFlex II, RigakuCo.) with CuKα (λ = 1.5418 Å) radiation (cathode voltage: 30 kV, current: 15 mA). An absorption spectrum was acquired at room temperature with a UV–vis spectrometer (UV-2600, Shimadzu Co.). Mott–Schottky analysis was carried out by using an electrochemical analyzer (604D, ALS Co.) with electrodes of gl-C_3N_4 doped with or not doped with boron atoms, a platinum electrode, an Ag/AgCl electrode and non-CO_2 bubbled 0.5 M $NaHCO_3$ solution (pH 8.6) used as a working electrode, counter electrode, reference electrode and electrolyte, respectively. X-ray photoelectron

spectroscopy (XPS) measurements were also performed using a Kratos AXIS Nova spectrometer (Shimazu Co. Ltd.) with a monochro-matic Al Kα X-ray source. The binding energy was calibrated by taking the carbon (C) 1s peak of contaminant carbon as a reference at 248.7 eV.

2.3. Photoelectrochemical measurements

Linear sweep voltammetry and chronoamperometry measurements were carried out by using an automatic polarization system (HSV-100, Hokuto Denko Co.) with a three-electrode system, in which the prepared electrode, a glassy carbon electrode and a silver–silver chloride (Ag/AgCl) electrode were used as a working electrode, counter electrode and reference electrode, respectively. The electrolyte used was 0.5 M $NaHCO_3$ solution, which was bubbled with CO_2 gas for 30 min to remove dissolved air. The pH of 0.5 M $NaHCO_3$ solution after bubbling with CO_2 gas for 30 min was pH 7.3. It should be noted that the CO_2 gas continuously flowed into the reactor during the linear sweep. The light source used was an AM 1.5 G solar-simulated system (PEC-L15, Peccell Tech., Inc.). The light intensity of the solar-simulated light was adjusted to 100 mW/cm^2 by utilizing a thermopile power meter (ORION-TH).

2.4. Evaluation of reduction products

Photoelectrochemical reduction of CO_2 to CO and C_2H_5OH over the electrodes of g-C_3N_4 doped with or not doped with boron atoms was carried out by using an automatic polarization system (HSV-100, Hokuto Denko Co.) with a three-electrode photoelectrochemical cell system in which electrodes of g-C_3N_4 doped with or not doped with boron atoms, a glassy carbon electrode and silver–silver chloride (Ag/AgCl) electrode were used as a working electrode, counter electrode and reference electrode, respectively. After CO_2 bubbling for 30 min, the cell was sealed and irradiated by AM 1.5 G solar-simulated light for 120 min. The gaseous CO_2 reduction products including CO, CH_4 and H_2 were detected by gas chromatography (490 Micro GC, Agilent Technology Co.). The CO_2 reduction product in aqueous phase (formic acid (HCOOH)) was detected by using single-channel ion chromatography (ICS900, Thermo Fisher Scientific Inc.). Other products including methanol (CH_3OH), ethanol (C_2H_5OH), and formaldehyde (HCOH) were detected by gas chromatography (G-3500, Hitachi Co.) with a DB-WAXetr column (122-7332, Agilent Co.).

2.5. Labeling CO_2 reduction experiments using $^{13}CO_2$

Degas and purge $^{13}CO_2$ processes are shown in Fig. S1.

After complete degassing the whole photoelectrochemical system described in section 2.3 by a diaphragm pump (Process 1), $^{13}CO_2$ gas was bubbled for 15 min (Process 2).

Photoelectochemical reduction of CO_2 was performed by irradiation of solar-simulated light at a potential of -0.4 V vs. Ag/AgCl for 120 min (Process 3). After the reaction, the aqueous samples (4 mL) for ^1H NMR were dissolved in D_2O (1 mL). 3-(Trimethylsilyl)-1-propanesulfonic acid sodium salt (Sigma–Aldrich) was used as an internal standard compound.

3. Results and discussion

3.1. Characterization

Figure 1 shows a diffuse reflectance spectrum of g-C_3N_4 doped with or not doped with boron atoms (g-C_3N_4 and BCNx, X= 0.5 − 3.0 at%). These photocatalysts exhibited visible-light absorption, and their absorption edges were around 550 nm. The band gap was found by extrapolation of the absorption bandedge, and it was estimated to be 2.59 eV for $BCN_{1.5}$.

The XRD pattern (Fig. 2) for all g-C_3N_4 derivatives including BCNx compounds showed their graphite stacking structures. The two diffraction peaks at 2θ = 13.18 and 27.48 match well with the (1 0 0) and (0 0 2) crystal planes of layered g-C_3N_4 [44]. The rather strong diffraction peak at 2θ = 27.48 is a characteristic indicator of layered stacking with a distance of 0.326 nm, and the in-planar repeating tri-s-triazine unit with a period of 0.675 nm can be clearly observed from the diffraction peak at 2θ =

13.18, which is consistent with the reported results for g-C_3N_4 [45]. In addition, peak intensities were gradually decreased by incorporation of boron atoms in the lattice of g-C_3N_4. The results of XRD analyses indicated that the particle sizes gradually decrease by the amount of boron atoms in the lattice of g-C_3N_4. These results suggested that lower crystallinity might be exhibited by introduction of boron atoms in the lattice of g-C_3N_4. The average crystal sizes were calculated by using Scherrer's formula to be 2.9, 2.1, 1.4, and 0.8 nm for g-C_3N_4, $BCN_{0.5}$, $BCN_{1.5}$, and $BCN_{3.0}$ according to the (0 0 2) peaks in the XRD patterns, respectively. XPS analysis of BCNx was performed as shown in Fig. 3. A peak was observed at 191.1 eV, which is assigned to boron atoms in the lattice of g-C_3N_4. This result is in good agreement with a previously reported result [39].

The conduction band potential of g-C_3N_4 was reported to be −1.35 V vs. Ag/AgCl [46-48]. To clarify the flat band potential (E_{fb}) of $BCN_{1.5}$, Mott–Schottky analyses were carried out by using an alternating current (AC) electrochemical impedance method at 0.1 kHz, 0.5 kHz and 1 kHz with AC 5 mV of amplitude in a non-CO_2 bubbled 0.5 M $NaHCO_3$ solution (pH 8.4). A Mott-shottky plot of $BCN_{1.5}$ in shown in Fig. 4. Negative slopes at all AC frequencies were obtained, indicating that $BCN_{1.5}$ behaves as a p-type semiconductor.

In the case of p-type semiconductors, E_{fb} is generally located near the VB, and it can be estimated from the intersection of a plot of $1/C^2$ against E by the following equation [49]:

$$\frac{1}{C^2} = \frac{2}{e\epsilon\epsilon_0 N}\left(E - E_{fb} - \frac{kT}{e}\right),$$

where C is capacitance, e is the electron charge, ϵ is the dielectric constant, ϵ_0 is permittivity of vacuum, N is acceptor density, E is the electrode potential, E_{fb} is the flat band potential, k is the Boltzmann constant, and T is temperature.

As shown in Fig. 4, the x-axis intersection was E = +1.53 V versus Ag/AgCl (pH 8.4) for all frequencies (0.1 kHz, 0.5 kHz, and 1 kHz) and can be used to determine E_{fb} from the above equation $E = E_{fb} - kT/e$. This calculation showed that E_{fb} was approximately +2.19 V v.s. NHE (pH 0) by correcting the solution pH. This result indicated that the VB potential and CB potential of p-type $BCN_{1.5}$ are approximately +2.19 V and −0.44 V v.s. NHE at pH 0, respectively. Fig. 5 shows a band potential diagram for g-C_3N_4 and $BCN_{1.5}$ together with the thermodynamic potentials for CO_2 reduction to various reduction products versus NHE at pH 0. As shown in this figure, the CB potential of p-type $BCN_{1.5}$ was high enough for CO_2 reduction to produce several kinds of products. Although the conduction band potential of $BCN_{1.5}$ was rather positive compared to that of g-C_3N_4, p-type properties of $BCN_{1.5}$ might be effective for CO_2 reduction.

3.2. Photoelectrochemical reduction of CO_2 over g-C_3N_4 and BCNx electrodes

Figure 6 shows linear sweep voltammetry of the BCNx photocathode as well as g-C_3N_4 in 0.5 M $NaHCO_3$ solution. After CO_2 gas had been continuously passed through for 1 h, the electrode was irradiated with AM 1.5 G solar-simulated light for estimation of photocurrent response. The p-type BCNx photocathode exhibited a larger cathodic photocurrent than that of n-type g-C_3N_4 in response to irradiation of solar light. The cathodic photocurrent density of BCNx with an optimum amount (x = 3.0) of boron doping reached 6.0 $\mu A/cm^2$ at −0.40 V applied potential vs. Ag/AgCl. The onset potential of the p-type $BCN_{3.0}$ photocathode was estimated to be approximately 0.15 V vs. Ag/AgCl (pH 7.3).

Figure 7 shows the time dependence of a cathodic photocurrent of the g-C_3N_4 and BCNx electrodes in 0.5 M $NaHCO_3$ solution (pH = 7.3) bubbled with CO_2 gas at −0.40 V applied potential vs. Ag/AgCl. When AM 1.5G solar-simulated light was irradiated to the g-C_3N_4 and BCNx electrodes, the cathodic photocurrent rapidly increased at the initial stage and then became relatively stable with time (longer than 30 min). The XRD pattern of the p-type g-C_3N_4 and BCNx photocathodes barely changed after the chronoamperometry measurement (not shown here). This result indicates that photocorrosion or reduction of the p-type g-C_3N_4 and BCNx photocathodes themselves might not occur. Therefore, the $BCN_{3.0}$ electrode was used for product analyses of photoelectrochemical CO_2 reduction.

After 30-min photoelectrochemical reduction of CO_2 using the g-C_3N_4 and $BCN_{3.0}$ electrodes, products as a result of CO_2 reduction were analyzed by Micro GC, Capillary GC and Ionic chromatography. The main product of CO_2

photoelectrochemical reduction over the $BCN_{3.0}$ electrode was ethanol (C_2H_5OH). CO was also detected as a minor product. The amounts of ethanol and CO were 73 nmol and 9 nmol, respectively. In photoelectrochemical reaction systems, CO_2 reduction usually competes with H_2 evolution as a result of H^+ reduction. Although the conduction potential of the $BCN_{3.0}$ electrode is sufficient to reduce H^+ to generate hydrogen, CO_2 reduction might preferably proceed because of hydrophobicity on the surface of the g-C_3N_4 and BCNx electrodes. The carbon source of ethanol will be discussed later on the basis of results of isotope experiments.

3.3. Effect of co-catalyst loading on photoelectrochemical activity

For further improvement of photoelectrochemical CO_2 reduction, Ag, Rh or Au nanoparticles as co-catalysts were loaded on the prepared $BCN_{3.0}$ electrode by the magnetron sputtering method. The thickness of these co-catalyst materials was adjusted to 1.0 nm by the optimized sputtering condition.

After loading the co-catalysts by the magnetron sputtering technique, the color of the samples changed depending on the kind of loading material. The colors of Rh-loaded, Ag-loaded and Au-loaded electrodes were pale silver, silver, and pale reddish silver, respectively. Figures 8 and 9 show linear sweep voltammetry and chronoamperometry with the photocurrent response of $BCN_{3.0}$ loaded with or not loaded with Au, Ag, or Rh as a co-catalyst. Photogenerated electrons in the photocatalysts

migrate to the co-catalyst such as Rh, Au, or Ag and reduced the adsorbed compounds such as CO_2.[50]

Figure 10 shows C_2H_5OH and CO generation as a result of photoelectrochemical reduction of CO_2 using the prepared g-C_3N_4 and $BCN_{3.0}$ electrodes with or without an optimum amount of Ag, Rh or Au loading. In addition Faraday efficiency of the products by CO_2 reduction were summarized in Table 1. As shown in Fig. 10, C_2H_5OH was observed as the main product. In addition, no hydrogen evolution was detected. The amount of C_2H_5OH drastically increased with co-catalyst loading. Among the three kinds of co-catalysts, Au showed the highest activity. These results indicated that loading an optimum amount of a co-catalyst on the surface of the $BCN_{3.0}$ electrode improves the photocatalytic activity for CO_2 reduction. Although the key mechanism for highly selective CO_2 reduction on the co-catalyst-loaded $BCN_{3.0}$ electrode is under investigation, preferential CO_2 adsorption on a co-catalyst loaded on the surface of the $BCN_{3.0}$ electrode might be one of the key steps for improving predominant CO_2 reduction. The increase in C_2H_5OH generation on the $BCN_{3.0}$ electrode loaded with a co-catalyst was presumably due to prevention of recombination and/or enhancement of selectivity for C_2H_5OH generation as a result of multi-electron reduction by electron capturing on metal particles. This effect probably depended on properties of co-catalyst particles, e.g., loading site, amount, particle size and dispersibility. Therefore, an excess amount of co-catalyst loading may result in loss of appropriate properties as co-catalyst particles, such as dispersibility and particle size.

3.4. Labeling experiments using $^{13}CO_2$ reduction of CO_2

We applied ^{1}H-NMR spectroscopy for analyzing the carbon source of C_2H_5OH as a main product for photoelectrochemical reduction of CO_2 using g-C_3N_4 or BCNx electrodes. A labeling experiment using $^{13}CO_2$ for CO_2 reduction was conducted over an Au-loaded $BCN_{3.0}$ electrode for 30 min under solar-simulated light irradiation. Before evaluation of the photoelectrochemical efficiency, the electrode was irradiated with UV light using black light (UVP, XX-15BLB) for one day in order to remove organic contaminats on the surface of the electrode. $^{1}O_2$ (15 mM) treatment of the electrode was performed for 2 h by using a $^{1}O_2$ generator (EKBIO-1100, Ebara Jitsugyo Co. Ltd) just before experiments on photoelectrochemical reduction of CO_2. Degasification and purge $^{13}CO_2$ processes are shown in Fig. S1.

$BCN_{3.0}$ loaded with Au was used for $^{13}CO_2$ reduction. After bubbled completely degassing the whole system by using a diaphragm pump (Process 1), $^{13}CO_2$ gas was bubbled for 15 min (Process 2). Photoelectrochemical CO_2 reduction was performed for 30 min during AM 1.5 solar-simulated light irradiation (Process 3). After the reaction, the aqueous samples (4 ml) for ^{1}H-NMR were dissolved in D_2O (1 ml). 3-(Trimethylsilyl)-1- propanesulfonic acid sodium salt (SIGMA-ALDRICH) was used as an internal standard compound. In the ^{1}H-NMR of the same solution, a double triplet attributable to the proton of the methyl group coupled to ^{13}C of $^{13}CH_3-$ and $-^{13}CH_2O-$ was observed at 1.041 and 1.292 ppm, but no triplet due to the proton of

$^{12}CH_3-$ was detected (Fig. 11). Furthermore, a double quartet assigned to the proton of the methylene group was observed at 3.493 and 3.780 ppm, which were coupled to ^{13}C of $^{13}CH_3-$ and $-^{13}CH_2O-$. These results clearly show that the carbon source of CH_3CH_2OH is $^{13}CO_2$.

4. Conclusion

We successfully developed a boron-doped g-C_3N_4 (BCNx) photocathode prepared by classical carbon nitride condensation. The BCNx photocathode exhibited a relatively stronger cathodic photocurrent compering to that of g-C_3N_4 not doped with boron with irradiation of AM 1.5 G solar-simulated light.

A thin film electrode of boron-doped g-C_3N_4 (BCNx) was succesfully prepared by electrophoretic technique. Although g-C_3N_4 had been reported to be n-type semiconductor, the property of BCNx was confirmed to be p-type semiconductor by Mott-Schottky analyses. The photocurrent response of the BCNx electrode for CO_2 reduction was enhanced by boron doping. C_2H_5OH was obtained as a main product. In addition, activity for photoelectrochemical CO_2 reduction by BCNx was enhanced by co-catalyst loading including Au, Ag or Rh by the sputtering technique. The carbon source of C_2H_5OH, which is the main product of CO_2 reduction using photoelectrochemical system with Au loaded $BCN_{3.0}$, was confirmed by a labeling experiment using $^{13}CO_2$.

Acknowledgments

This work was supported by JST PRESTO program and JST ACT-C program.

Figure Captions

Figure 1. Diffuse reflectance spectrum of g-C_3N_4 doped with or not doped with boron atoms.

Figure 2. XRD patterns of g-C_3N_4 doped with or not doped with boron atoms.

Figure 3. XPS spectrum of $BCN_{3.0}$.

Figure 4. Mott-shottky plot of $BCN_{1.5}$.

Figure 5. Band potential diagram for g-C_3N_4 and $BCN_{1.5}$ together with the thermodynamic potentials for CO_2 reduction to various reduction products versus NHE at pH 0.

Figure 6. Linear sweep voltammetry of the g-C_3N_4 and BCNx electrodes.

Figure 7. Time dependence of a cathodic photocurrent (chronoamperometry) of the g-C_3N_4 and BCNx electrodes.

Figure 8. Linear sweep voltammetry of the $BCN_{3.0}$ electrodes loaded with or not loaded with co-catalysts.

Figure 9. Chronoamperometry of the $BCN_{3.0}$ electrodes loaded with or not loaded with co-catalysts.

Figure 10. Products analyses of photoelectrochemical reduction of CO_2 over

co-catalyst loaded $BCN_{3.0}$ electrodes

Figure 11. ^{1}H-NMR spectra of the ethanol produced by photoelectrochemical reduction of $^{13}CO_2$ using Au-loaded $BCN_{3.0}$ electrodes.

Figure S1. Process of photoelectrochemical CO_2 reduction using $^{13}CO_2$

References

[1] O.K. Varghese, M. Paulose, T.J. LaTempa, C.A. Grimes, Nano Lett. 9 (2009) 731–737.

[2] A. J. Morris, G. J. Meyer, E. Fujita, Acc. Chem. Res. 42 (2009) 1983−1994.

[3] E. Fujita, Coord. Chem. Rev. 185 (1999) 373−384.

[4] H. Takeda, O. Ishitani, Coord. Chem. Rev. 254 (2010) 346−354.

[5] Y. T. Liang, B. K. Vijayan, K. A. Gray, M. C. Hersam, Nano Lett. 11 (2011) 2865−2870.

[6] C. W. Tsai, H. M. Chen, R. S. Liu, K. Asakura, T. S. Chan, J. Phys. Chem. C 115 (2011), 10180−10186.

[7] Y. Izumi, Coord. Chem. Rev. 257 (2013), 171−186.

[8] B. Aurian-Blajeni, M. Halmann, J. Manassen, Sol. Energy. Mater. 8 (1983), 425−440.

[9] E. E. Barton, D. M. Rampulla, A. B. Bocarsly, J. Am. Chem. Soc. 130 (2008) 6342−6344.

[10] M. Halmann, Nature 275 (1978) 115.

[11] S. Kaneco, H. Katsumata, T. Suzuki, K. Ohta, Chem. Eng. J. 116 (2006) 227−231.

[12] J.Y. Liu, B. Garg, Y.C. Ling, Green Chem. 13 (2011) 2029–2031.

[13] T. Inoue, A. Fujishima, S. Konishi, K. Honda, Nature 277 (1979) 637–638.

[14] F. Solymosi, I. Tomba´ cz, Catal. Lett. 27 (1994) 61–65.

[15] M. Anpo, H. Yamashita, Y. Ichihashi, Y. Fujii, M. Honda, J. Phys. Chem. B 101 (1997) 2632–2636.

[16] I. H. Tseng, J.C.S. Wu, H.Y. Chou, J. Catal. 221 (2004) 432–440.

[17] Q. H. Zhang, W.D. Han, Y.J. Hong, J.G. Yu, Catal. Today 148 (2009) 335–340.

[18] K. Koci, K. Mateju, L. Obalova, S. Krejcikova, Z. Lacny, D. Placha, L. Capek, A. Hospodkova, O. Solcova, Appl. Catal. B: Environ. 96 (2010) 239–244.

[19] T. Yui, A. Kan, C. Saitoh, K. Koike, T. Ibusuki, O. Ishitani, ACS Appl. Mater. Interfaces 3 (2011) 2594–2600.

[20] K. Sayama, H. Arakawa, Phys. Chem. 97 (1993) 531–533.

[21] Y. Matsumoto, M. Obata, J. Hombo, J. Phys. Chem. 98 (1994) 2950–2951.

[22] P.W. Pan, Y.W. Chen, Catal. Commun. 8 (2007) 1546–1549.

[23] Q. Liu, Y. Zhou, J. Kou, X. Chen, Z. Tian, J. Gao, S. Yan, Z. Zou, J. Am. Chem. Soc. 132 (2010) 14385–14387.

[24] S. C. Yan, S.X. Ouyang, J. Gao, M. Yang, J.Y. Feng, X.X. Fan, L.J. Wan, Z.S. Li, J.H. Ye, Y. Zhou, Z.G. Zou, Angew. Chem. Int. Ed. 49 (2010) 6400–6404.

[25] Y. Zhou, Z. Tian, Z. Zhao, Q. Liu, J. Kou, X. Chen, J. Gao, S. Yan, Z. Zou, ACS Appl. Mater. Interfaces 3 (2011) 3594–3601.

[26] K. Iizuka, T. Wato, Y. Miseki, K. Saito, A. Kudo, J. Am. Chem. Soc. 133 (2011) 20863–20868.

[27] T. Ohno, N. Murakami, T. Koyanagi, Y. Yang , J. CO_2 utilization, 6 (2014) 17–25.

[28] K. Maeda, X. Wang, Y. Nishihara, D. Lu, M. Antonietti, K. Domen, J. Phys. Chem. C133 (12) (2009) 4940–4947.

[29] S. C. Yan, Z.S. Li, Z.G. Zou, Langmuir 25 (17) (2009) 10397–10401.

[31] J. Mao, T. Peng, X. Zhang, K. Li, L. Ye, L. Zan, Catal. Sci. Technol. 3 (2013) 1253–1260.

[30] J. Lin, Z. Pan, X. Wang, ACS Sustain. Chem. Eng. 10 (2013) 1021.

[31] K. Maeda, K. Sekizawa, O. Ishitani, Chem. Commun. 49 (2013) 10127–10129.

[32] Z. Huang, F. Li, B. Chen, T. Lu, Y. Yuan, G. Yuan, Appl. Catal. B 136–137 (2013) 269–277.

[33] Y. Zheng, J. Liu, J. Liang, M. Jaroniec, S.Z. Qiao, Energy Environ. Sci. 5 (2012) 6717–6731.

[34] J. Zhang, M. Grzelczak, Y. Hou, K. Maeda, K. Domen, X. Fu, M. Antonietti, X. Wang, Chem. Sci. 3 (2012) 443–446.

[35] Y. Wang, X. Wang, M. Antonietti, Angew. Chem. Int. Ed. 51 (2012) 68–89.

[36] M. B. Ansari, B.H. Min, Y.H. Mo, S.E. Park, Green Chem. 13 (2011) 1416–1421.

[37] S. S. Park, S.W. Chu, C. Xue, D. Zhao, C.S. Ha, J. Mater. Chem. 21 (2011) 10801–10807.

[38] Q. Xiang, J. Yu, and M. Jaroniec, J. Phys. Chem., C, 115 (2011) 7355-7363.

[39] Y, Wang, H. Li, Jia Yao, Xinchen Wang and M. Antonietti, Chem. Sci., 2 (2011)

446–450.

[40] S. C. Yan, Z. S. Li, and Z. G. Zou, Langmuir, 26 (2010) 3894-3901.

[41] Y. Zhang, T. Mori, J. Ye, and M. Antonietti, J. Am, Chem. Soc., 132 (2010) 6294-6295.

[42] G. Liu, P. Niu, C. Sun, S. C. Smith, Z. Chen, G. Qing Lu, and H.-M. Cheng, J. Am, Chem. Soc., 132 (2010) 11642-11648.

[43] A. Thomas, A. Fischer, F. Goettmann, M. Autonietti, J.O. Mu¨ ller, R. Schlo¨ gl, J. M. Carlsson, J. Mater. Chem. 18 (2008) 4893–4908.

[44] X.C. Wang, K. Maeda, A. Thomas, K. Takanabe, G. Xin, J.M. Carlsson, K. Domen, M. Antonietti, Nat. Mater. 8 (2009) 76–80.

[45] F. Dong, L.W. Wu, Y.J. Sun, M. Fu, Z.B. Wu, S.C. Lee, J. Mater. Chem. 21 (2011) 15171–15174.

[46] J. Zhang, X. Cheng, K. Takanabe, K. Maeda, K. Domen, J. D. Epping, X. Fu, M. Antonietti, and X. Wang, Angew. Chem. Int. Ed. 49 (2010) 441 –444.

[47]. H. Zhang, L. H. Guo, L. Zhao, B. Wan, and Y. Yang, J. Phys. Chem. Lett. 6 (2015) 958−963.

[48] C. Ye, J. X. Li, Z. J. Li, X. B. Li, X. B. Fan, L. P. Zhang, B. Chen, C. H. Tung, and L. Z. Wu, ACS Catal. 5 (2015) 6973−6979.

[49] L. Kavan, M. Grätzel, S.E. Gilbert, C. Klemenz, H.J. Scheel, J. Am. Chem. Soc. 118 (1996) 6716.

[50] K. Maeda, K. Teramura, D. Lu, N. Saito, Y. Inoue, K. Domen, J. Phys. Chem. C, 111 (2007) 7554-7560.

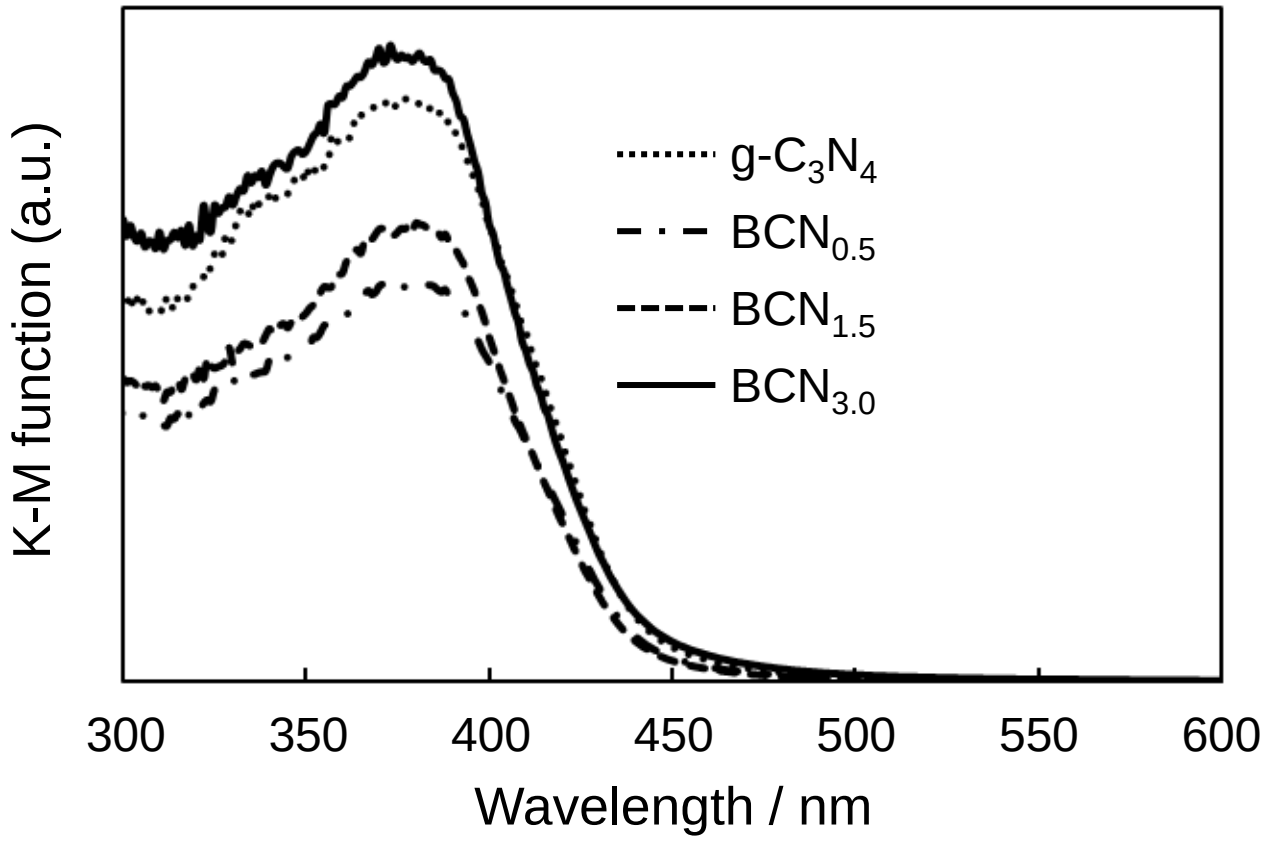

Figure 1. Diffuse reflectance spectrum of g-C3N4 doped with or not doped with boron atoms.

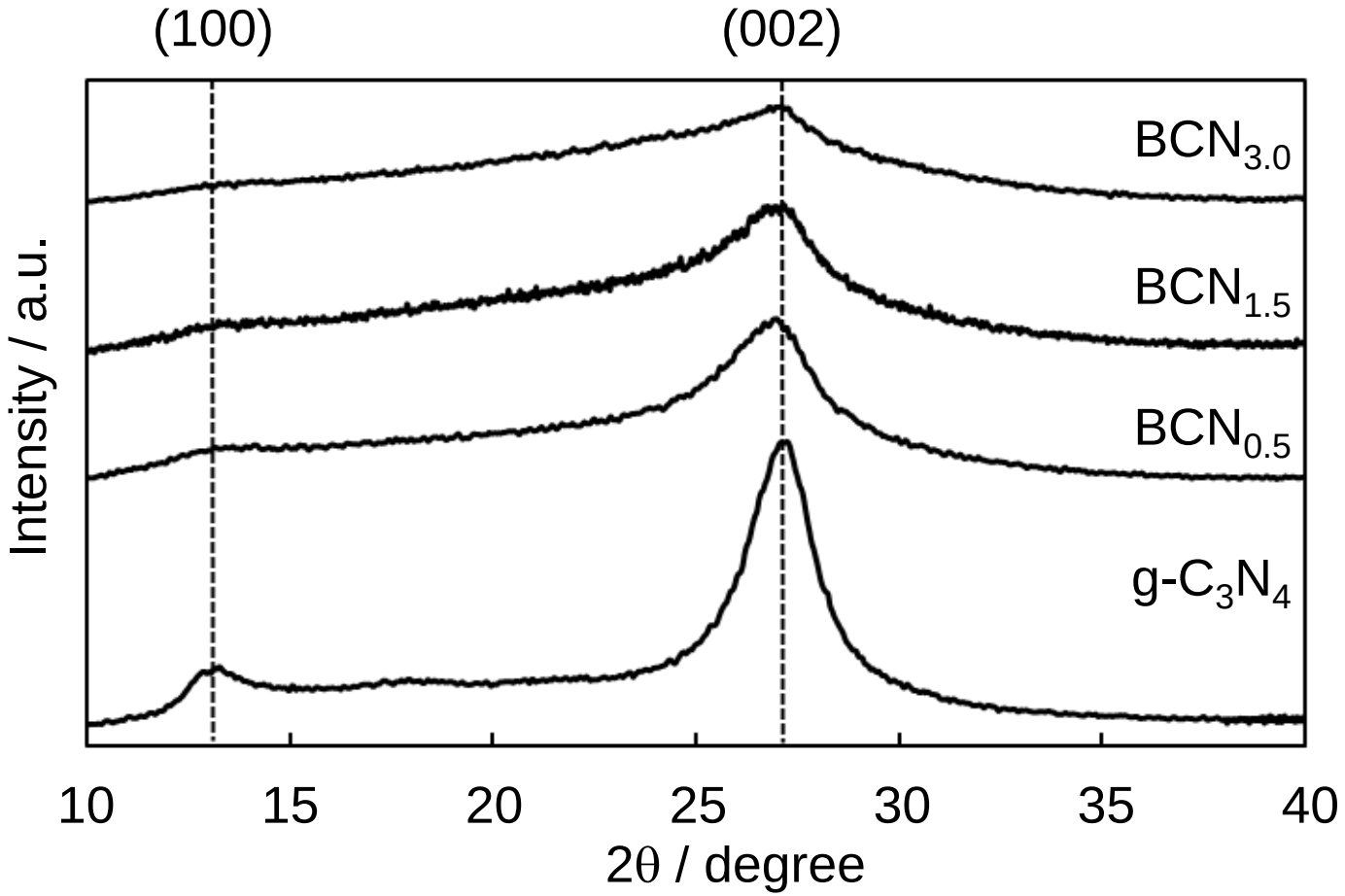

Fig. 2. XRD patterns of g-C3N4 doped with or not doped with boron atoms.

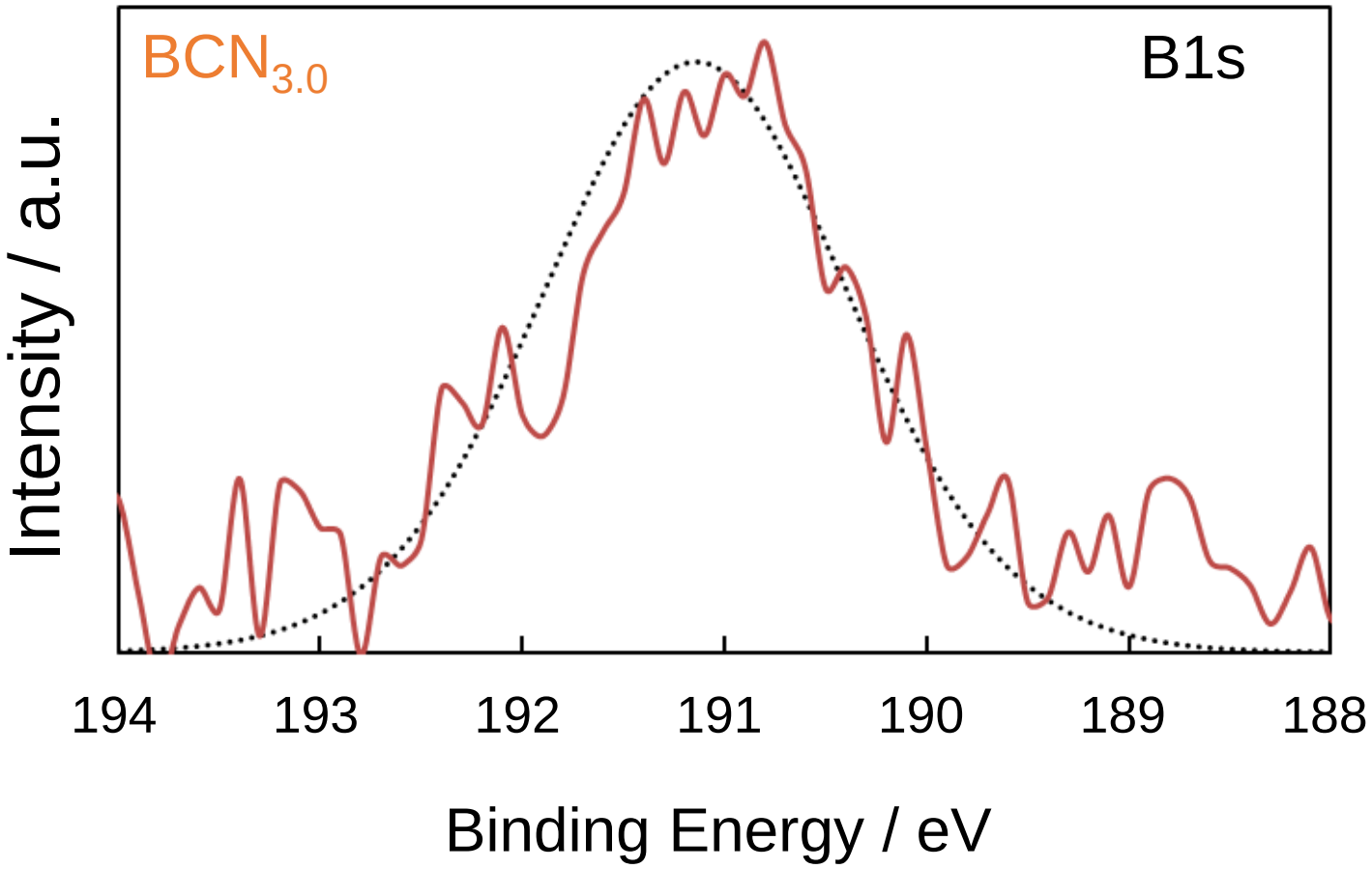

Fig. 3. XPS spectrum of BCN3.0.

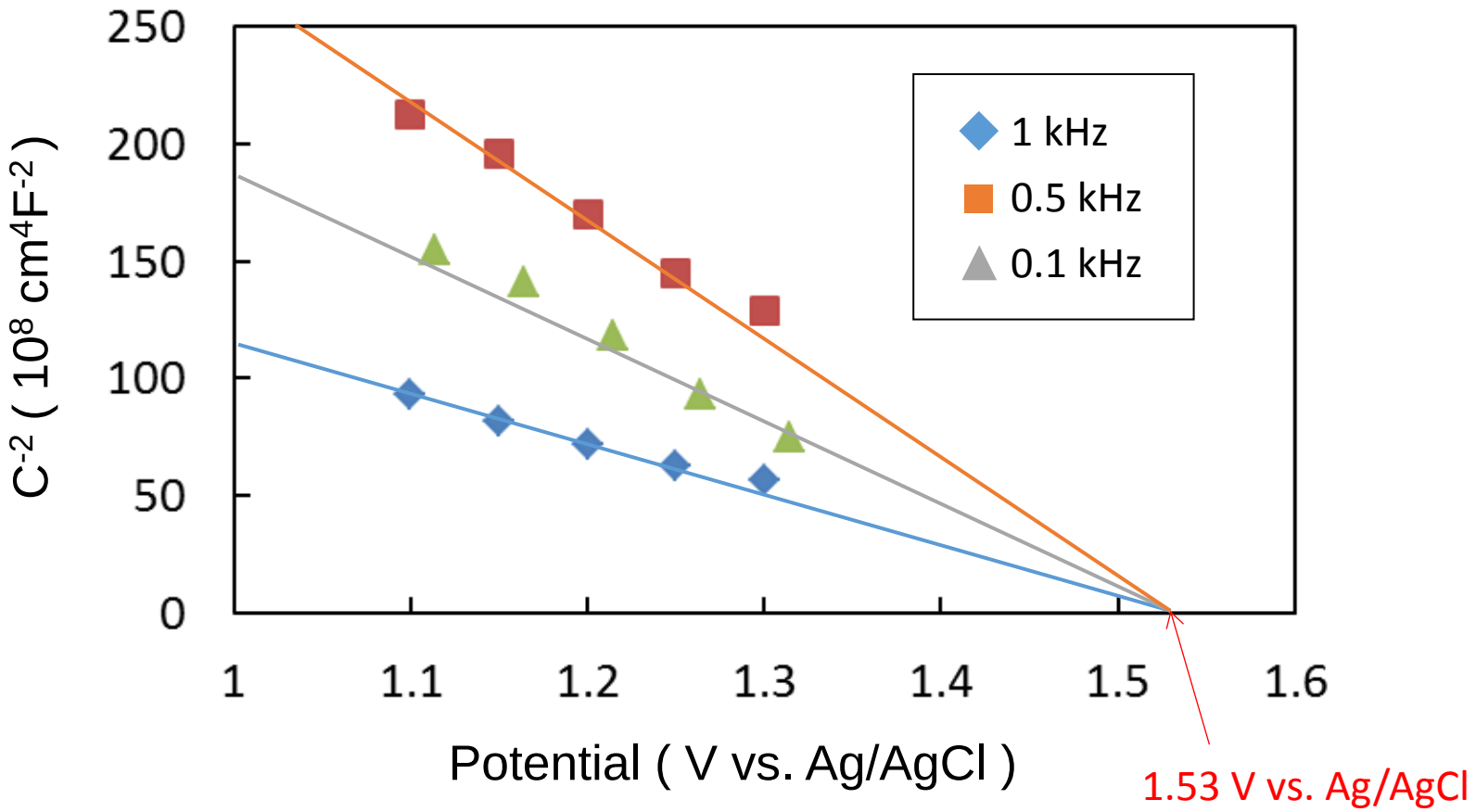

Fig. 4. Mott-shottky plot of BCN1.5.

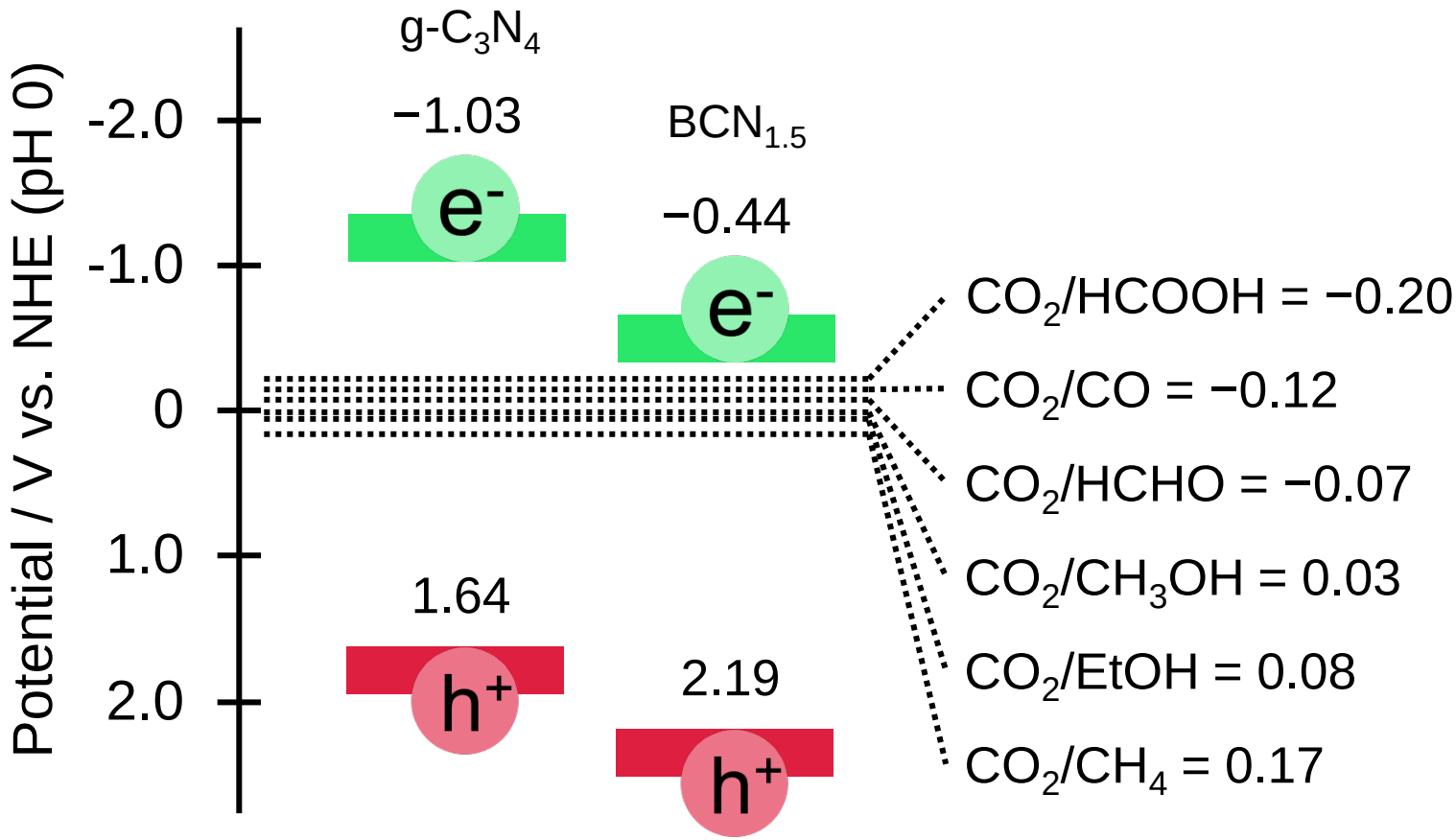

Fig. 5. Band potential diagram for g-C3N4 and BCN1.5 together with the thermodynamic potentials for CO2 reduction to various reduction products vs. NHE at pH 0.

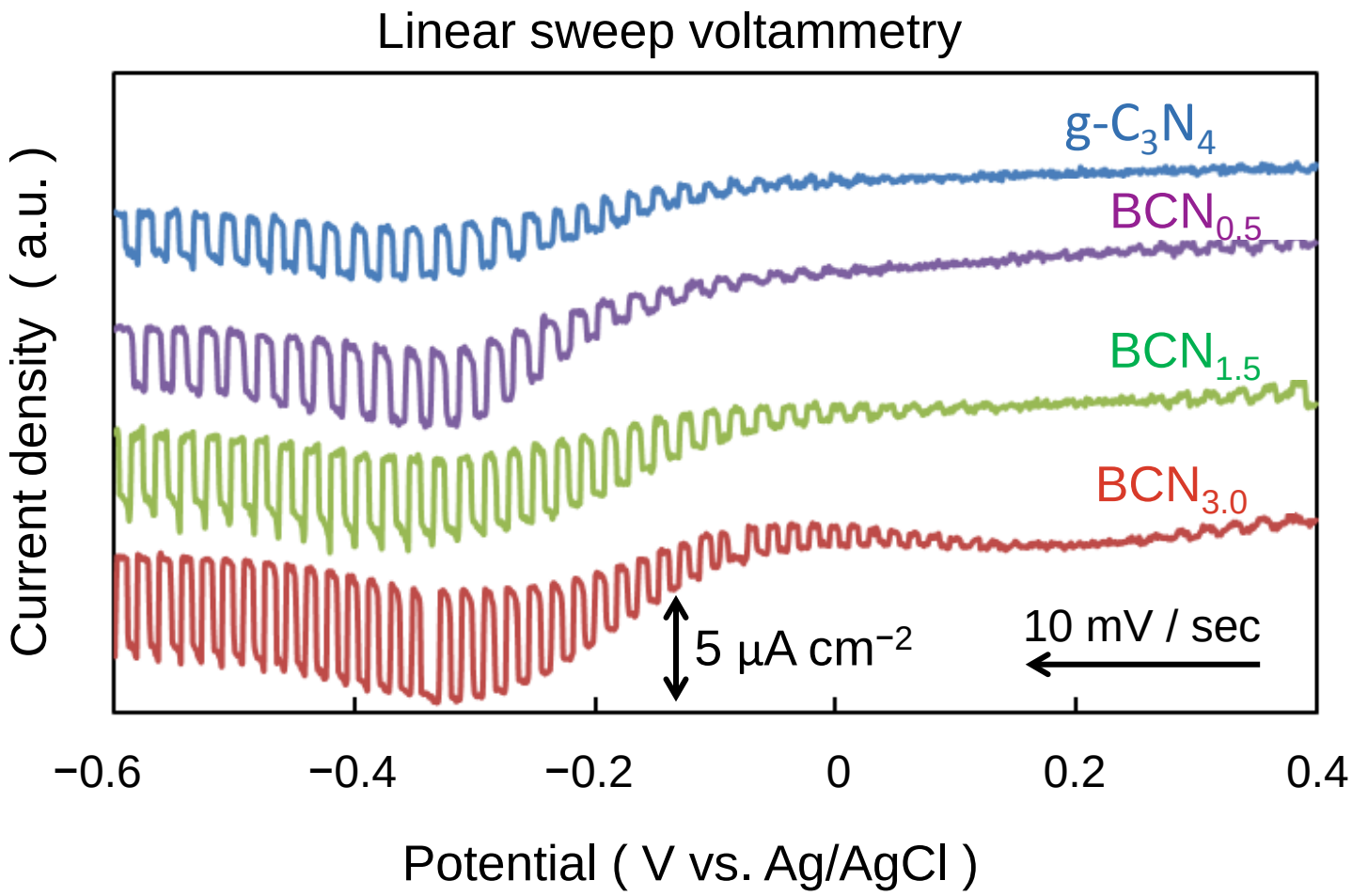

Fig. 6. Linear sweep voltammetry of the g-C3N4 and BCNx electrodes.

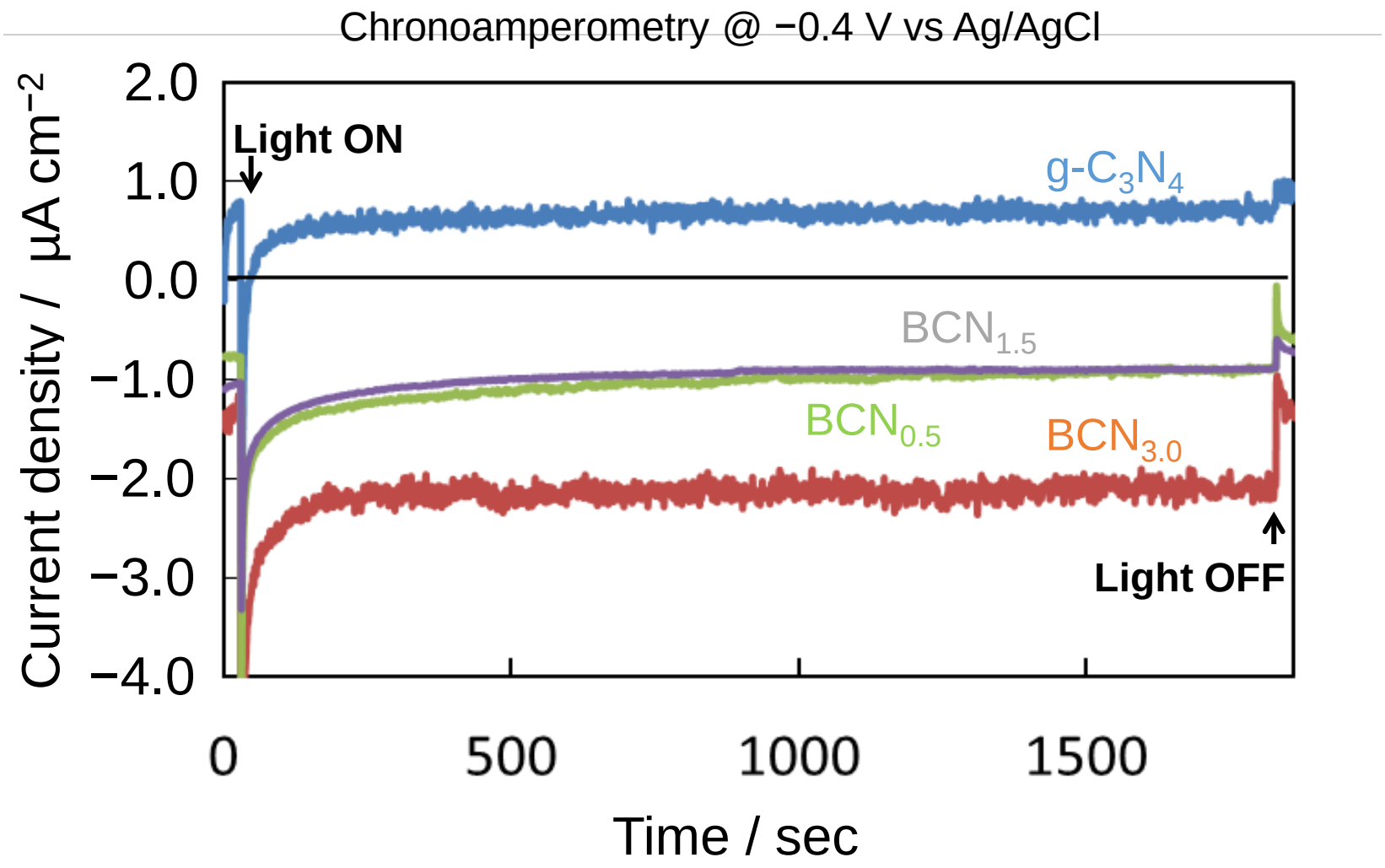

Fig. 7. Time dependence of a cathodic photocurrent (chronoamperometry) of the g-C3N4 and BCNx electrodes.

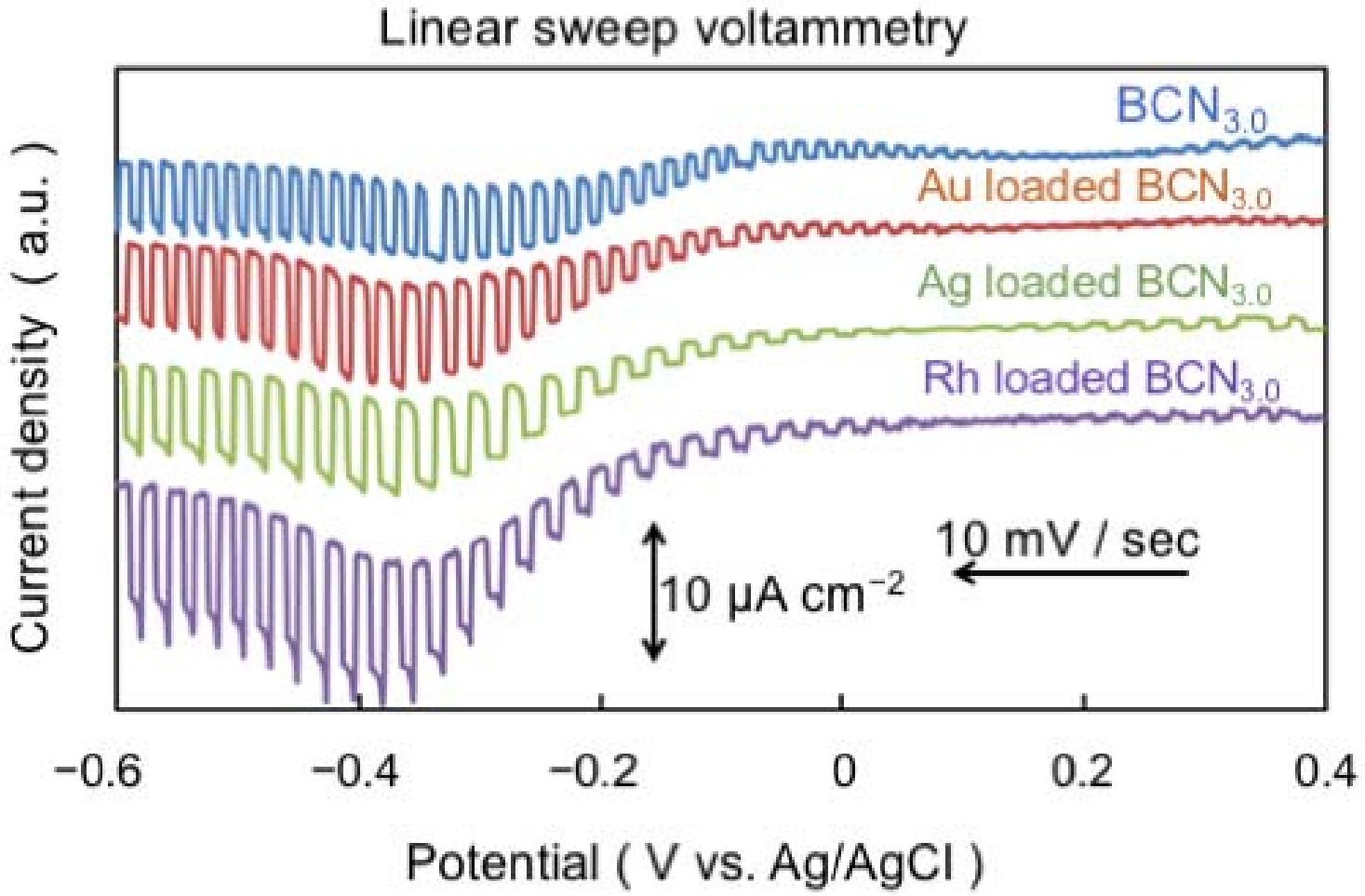

Figure 8. Linear sweep voltammetry of the BCN3.0 electrodes loaded with or not loaded with co-catalysts.

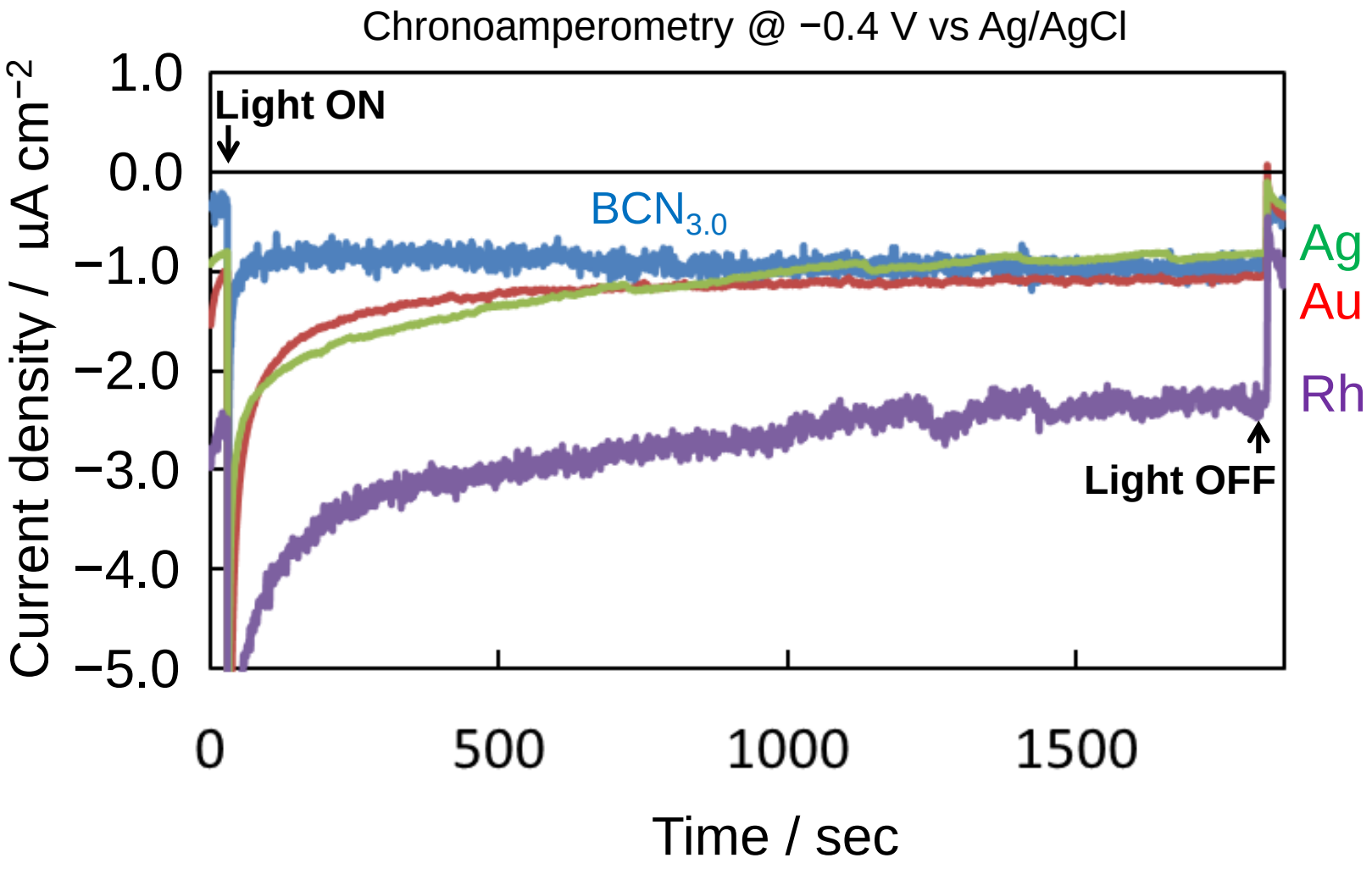

Fig. 9. Chronoamperometry of the BCN3.0 electrodes loaded with or not loaded with co-catalysts.

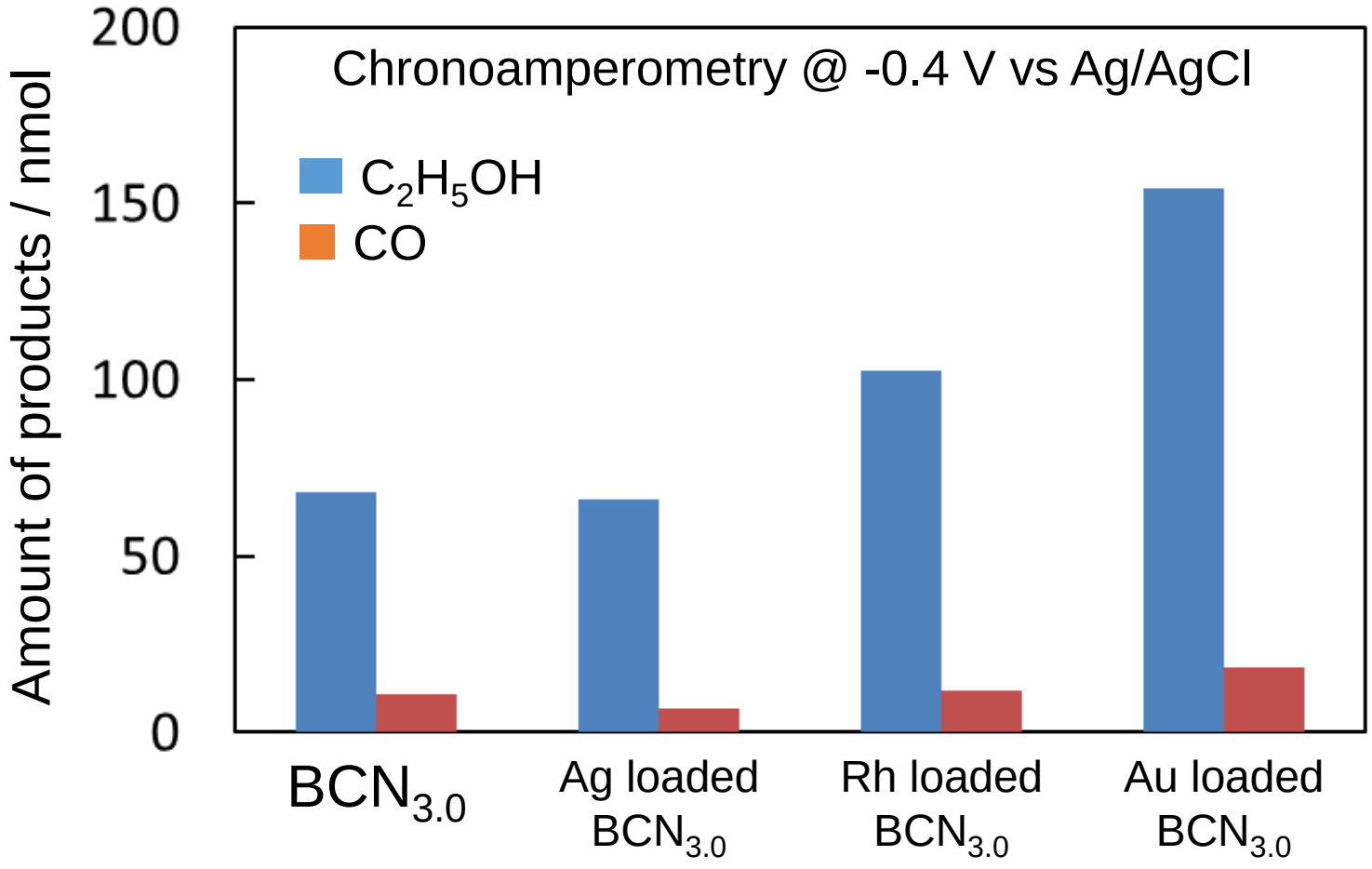

Fig. 10. Products analyses of photoelectrochemical reduction of CO2 over co-catalyst loaded BCN3.0 electrodes.

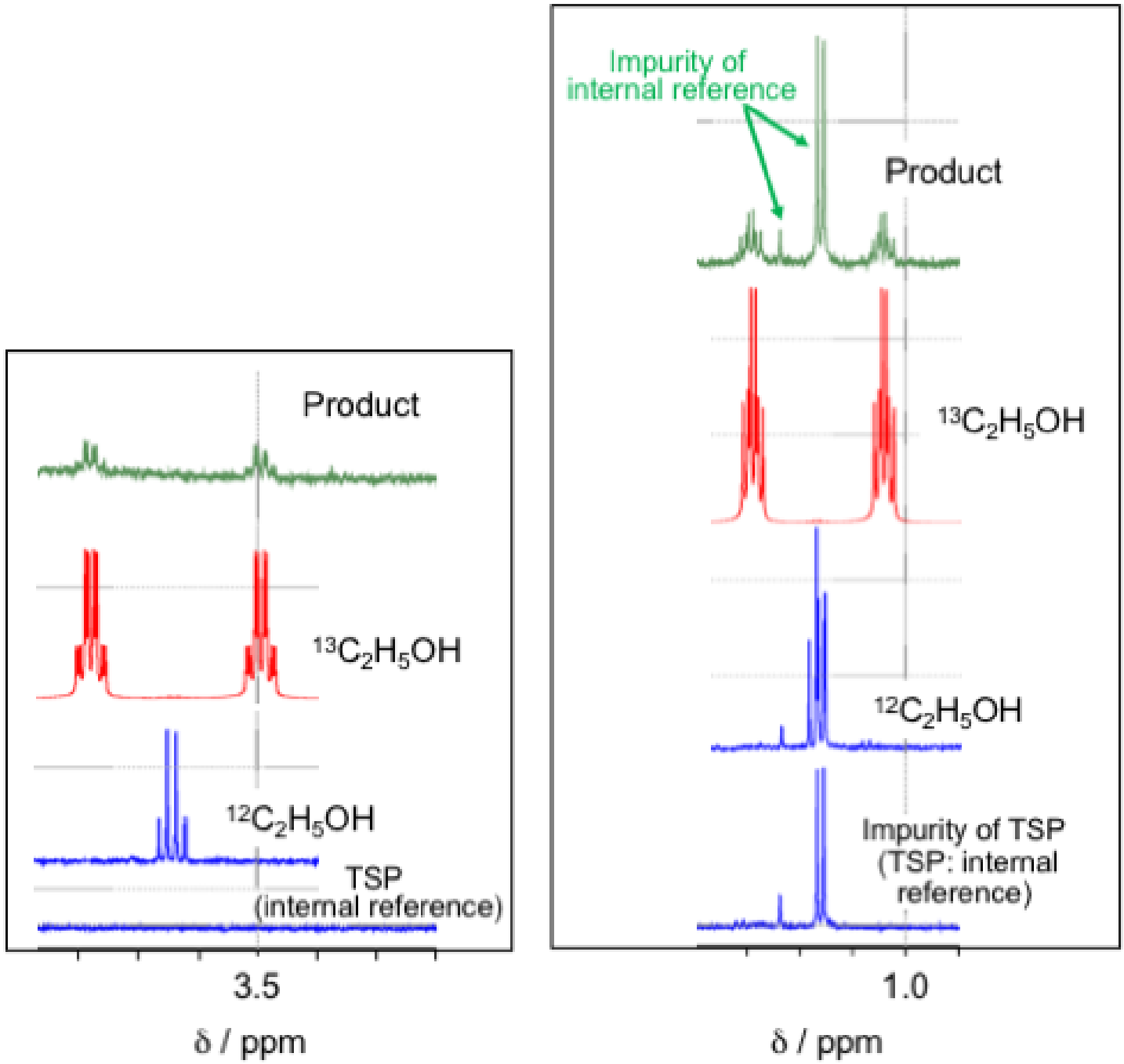

Figure 11. 1H-NMR spectra of the ethanol produced by photoelectrochemical reduction of 13CO2 using Au-loaded BCN3.0 electrodes.

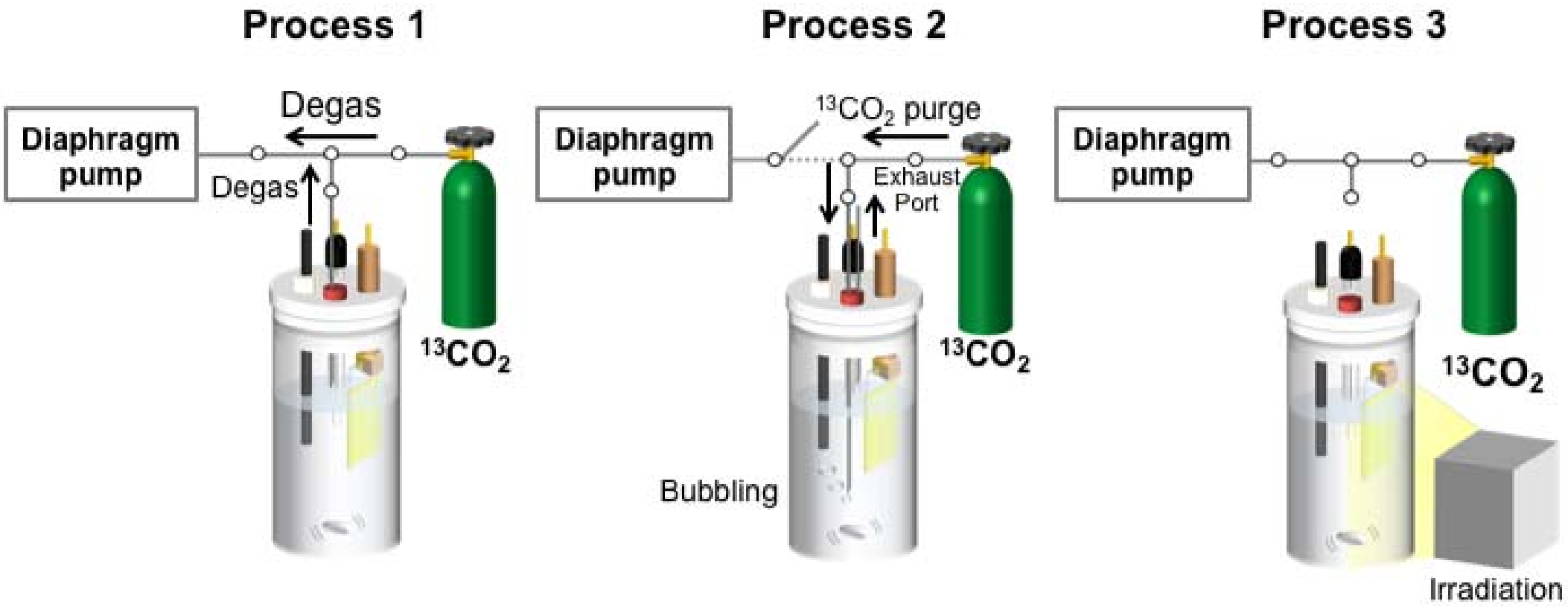

Figure S1. Appendix A. Supplementary data

Table 1
Faraday efficiency of the products.

	Faraday efficiency/%			
	$BCN_{3.0}$	Ag loded $BCN_{3.0}$	Rh loaded $BCN_{3.0}$	Au loaded $BCN_{3.0}$
EtOH	78	73	36	47
CO	1.2	1.2	0.7	0.9